TITLE:

Facile strategy for obtaining luminescent polymorphs based on the chirality of a boron-fused azomethine complex

AUTHOR(S):

Ohtani, Shunsuke; Takeda, Yusuke; Gon, Masayuki; Tanaka, Kazuo; Chujo, Yoshiki

京都大学
KYOTO UNIVERSITY

COMMUNICATION

Facile Strategy for Obtaining Luminescent Polymorphs Based on Chirality of Boron-Fused Azomethine Complex
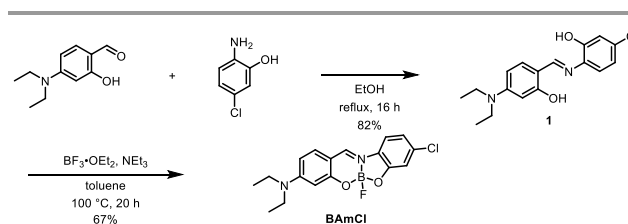
Shunsuke Ohtani, Yusuke Takeda, Masayuki Gon, Kazuo Tanaka* and Yoshiki Chujo

A chloro-substituted boron-fused azomethine complex (BAmCl) having a stereogenic boron center was synthesized for obtaining a luminescent chiral crystal. We succeeded in isolating the (*R*)- and (*S*)-enantiomers of BAmCl and preparing the homochiral polymorphic crystal, while we obtained the racemic crystal with *rac*-BAmCl. Single crystal X-ray diffraction analyses suggest that a variety of intermolecular interaction patterns and intrinsic flexibility of the molecular framework should play a significant role in stabilizing the homochiral crystal. We found the difference in molecular arrangements between the racemic and the homochiral crystals, and we observed distinct different emission colors. In particular, we observed heat-initiated homogeneous racemization without the need for a solvent or catalyst in the molten state of the homochiral crystal (*R*)-BAmCl. Our results mean that chiral resolution of a flexible fused-skeleton having a stereogenic boron center can be a platform for creating luminescent polymorphic materials.

Organic chromophores with variable solid-state emission properties have gathered considerable attention as a platform for realizing advanced organic devices such as, luminescent sensors for monitoring slight environmental changes[1] and bioprobes for assessing biological events and reactions.[2] Recently, we developed various types of solid-state luminescent molecules with stimuli-responsivity based on the concept of "element-blocks", which are minimum functional units containing heteroatoms, to create functional luminescent materials.[3] In the series of studies, we discovered that boron-fused complexes with tridentate ligands exhibited superior solid-state emission and unique environment responsivity.[4] In particular, we found that the boron-fused azomethine complex **BAm** showed crystallization-induced emission (CIE) property[4a], where less-emissive molecules in solution are turned to be strongly emissive in crystal.[5] We revealed that the restriction of molecular motions is responsible for emission enhancement in solid. Interestingly, the two polymorphic crystals of **BAm** were obtained and their emissive colors were critically different.

Polymorphism alteration is currently recognized as a promising strategy to tune a crystalline-state emissive property and various types of optically-functional materials have been developed.[6] However, precise controls of polymorphism are extensively challenging because it is difficult to predict whether a newly synthesized compound is polymorphic or not. To propose one solve for this problem, we focus on the stereogenic boron center of **BAm**. According to the above-mentioned previous research, we obtained the two polymorphs as racemic crystals consisting of (*R*)- and (*S*)-enantiomers of **BAm**. In particular, conventional organic luminescent dyes usually show poor emission in solid due to concentration quenching originated form intermolecular interactions, meanwhile **BAm** can provide not only intense emission in crystal but also different luminescent colors between polymorphs. On the basis of these data, we assumed that another luminescent homochiral crystal would be available by the chiral resolution. However, according to the so-called Wallach's rule, homochiral crystals are empirically less stable than the corresponding racemic crystals due to the inefficient molecular packing.[7] In fact, our preliminary experiment suggested that the crystallinities of the separated **BAm** enantiomers were extremely poor, and we failed to get the homochiral crystal. Therefore, further elaboration must be required for preserving homochiral states.

a. *Department of Polymer Chemistry, Graduate School of Engineering, Kyoto University Katsura, Nishikyo-ku, Kyoto 615-8510, Japan. E-mail: tanaka@poly.synchem.kyoto-u.ac.jp*

b. †*Electronic Supplementary Information (ESI) available. See* DOI: 10.1039/x0xx00000x

Scheme 1. Synthetic route of **BAmCl**.

Although organoboron compounds have been considered to be a class of highly-efficient luminescent dyes, a large number of luminescent boron complexes are achiral or racemic mixtures.[8] Especially, there are only a few examples to be resolved despite the easy introduction of chiral elements into π-conjugated skeleton.[9] In this work, we synthesized a new **BAm** derivative with the chlorine substitution, which can provide additional intermolecular interactions to enhance the crystallinity of enantiopure samples. As a result, we succeeded in obtaining the homochiral crystal as well as the racemic crystal. From the result of a single crystal X-ray diffraction (SCXRD) analysis, it was proposed that a variety of the intermolecular interactions and the intrinsic flexibility of **BAm** framework contributed to the stabilization of the homochiral crystal. Moreover, these two crystals showed different emission colors dependent on the molecular arrangements. Additionally, in the homochiral crystal, the homogeneous racemization was observed through the molten state in the absence of any solvents and catalysts. To the best of our knowledge, this is the first example of homogeneous racemization in the boron-centered chiral compounds.

The synthetic route to **BAmCl** is shown in Schemes 1 and S1–S2. The chlorine-substituted azomethine ligand **1** was prepared by a conventional condensation reaction (82% isolated yield). Subsequently, **BAmCl** was obtained from **1** as a racemic mixture by boron complexation in 67% isolated yield. The structure of **BAmCl** was examined by ^1H, ^{11}B, ^{13}C NMR, ionization mass measurements and elemental analyses (Fig. S1–S8), and we concluded the desired molecule was obtained with high purity. The chiral resolution of the racemic mixture of **BAmCl** was carried out through chiral high-performance liquid chromatography (HPLC) using an amylose-based stationary phase with *n*-hexane/THF (v/v = 1/3) as an eluent (See Table S1 for detail analysis condition). The chiral HPLC profile showed the two peaks attributable to (*R*)- and (*S*)-enantioners (Fig. S9). From the peak integral ratios, it was found that **BAmCl** existed in racemic mixture with almost the same ratio (Peak 1: 51%, Peak 2: 49%).The two peaks were successfully resolved into two fractions, **BAmCl-fr1** and **BAmCl-fr2**, with the retention times of 57.2 min and 62.6 min, respectively (flow rate: 3.5 mL/min). From the results of the enantiomer peak integrals, **BAmCl-fr1** and **BAmCl-fr2** were determined as >99% enantiomeric excess (ee) and 95% ee, respectively. The ee value of **BAmCl-fr2** was lifted to 97% after recrystallization. Fig. S10 shows the circular dichroism (CD) and UV–vis absorption spectra for **BAmCl-fr1** and **BAmCl-fr2**. The mirror image in CD spectra from both fractions means that the two fractions should be a pair of enantiomers. In order to ensure the stability of the chirality, the time-dependent CD measurement was conducted with the toluene solution of **BAmCl-fr1** at 80 °C (Fig. S11). Significant racemization was hardly observed even after heating for 4 h, suggesting that the chirality on the stereogenic boron center in the boron-fused azomethine complex system was enough stable to evaluate the properties under ambient conditions.

The SCXRD analysis elucidated that the racemic crystal obtained from *rac*-**BAmCl** belongs to the centrosymmetric space group $P2_1/c$ (Table S2). Fig. 1a represents the packing

mode of *rac*-**BAmCl** and the molecules show a dimeric motif of alternating adjacent (*R*)- and (*S*)-**BAmCl**. From the analyses of short contacts between the molecules, the existence of relatively strong halogen-based hydrogen bonds (CH···F or Cl) was proposed. In particular, the dimeric molecular motif was stabilized by the formation of two equivalent CH···F hydrogen bonding interactions between each molecule's fluorine atom and aromatic hydrogen atom (Fig. S12). By contrast, from the molecular arrangement of **BAmCl-fr1**, it was found that three (*R*)-**BAmCl** molecules formed helical stacking columns in the unit cell and CH···F hydrogen bonding interactions were observed among them (Fig. S13). The space group belongs to the noncentrosymmetric $P3_2$, indicating **BAmCl-fr1** crystalizes as a chiral crystal (Table S3). The Flack parameter was refined to 0.06(2), confirming the (*R*)-configuration at the boron stereocenter. From these results, the remaining **BAmCl-fr2** was assigned as (*S*)-**BAmCl** (hereinafter, the crystals obtained from **BAmCl-fr1** and **BAmCl-fr2** are called (*R*)-**BAmCl** and (*S*)-**BAmCl**, respectively). Moreover, the diethylamine groups CH···Cl hydrogen bonding were observed among the adjacent helical molecular columns, suggesting that the chlorine atom had some degree of contribution to stabilization of the chiral crystal structure (Fig. S13).

In both crystal structures, there seems to be subtle interfacial π–π interactions in the crystal packing owing to steric hindrance imposed by the distorted π-conjugated system and the protruded fluorine atom as we previously reported.[4] Meanwhile, CH···π interactions were also observed between multiple H atoms and two aromatic phenyl rings in addition to the halogen-based hydrogen bonding (Fig. S12 and S13). In comparison to the molecular structures of crystals, it is clearly shown that the dihedral angle between two phenyl groups totally differs among them (*rac*-**BAmCl**: 165.5°; (*R*)-**BAmCl**: 156.8°). These facts indicate that the boron-fused structure of **BAmCl** can adopt suitable molecular conformation dependent on molecular packings. In general, the conformational flexibility is advantageous for obtaining polymorphs because variable structures are acceptable in flexible molecules more than rigid ones.[10] In this regard, the flexible molecular framework of **BAmCl** should play a significant role in the formation of chiral
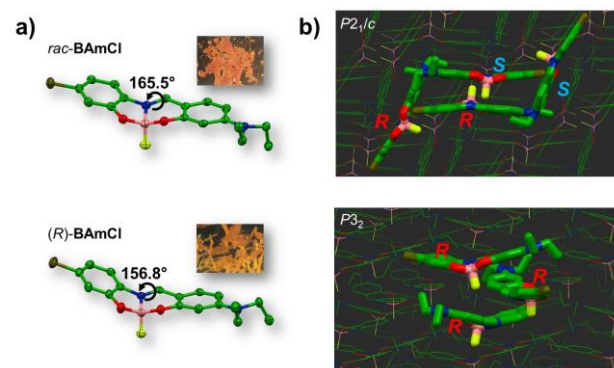

Fig. 1 a) Thermal ellipsoid (probability level 50%) and b) packing structures of *rac*-**BAmCl** and (*R*)-**BAmCl** (*green* carbon atoms; *blue* nitrogen atoms; *red* oxygen atoms; *pink* boron atoms; *yellow* fluorine atoms; *gold* chlorine atoms; hydrogen atoms are omitted for clarity).

Table 1 Optical properties of **BAmCl**

	$\lambda_{max,abs}$ (nm)[d]	λ_{em} (nm)[e]	Φ_F[f]	k_r (×10⁷s⁻¹)[g]	k_{nr} (×10⁸s⁻¹)[g]
Sol.[a]	445, 464	526	0.002	0.17	87
Amor.[b]	–	–	<0.001	–	–
rac-**BAmCl**[c]	–	585	0.37	4.0	6.6
(*R*)-**BAmCl**[c]	–	568	0.29	7.3	18

[a]1.0×10⁻⁵ M chloroform solution. [b]Amorphous sample prepared by a melt quenching method. [c]Crystalline sample. [d]The longest absorption maximum. [e]Fluorescence maxima with the excitation at the longest absorption maximum. [f]Absolute quantum efficiencies. [g]$k_r = \Phi_F/\tau_{av}$, $k_{nr} = (1 - \Phi_F)/\tau_{av}$, $\tau_{av} = \Sigma\alpha_i\tau_i^2/\Sigma\alpha_i\tau_i$

crystal as well as the stabilization effect by intermolecular interactions. Furthermore, it should be noted that the crystal densities were determined as 1.457 g cm⁻³ and 1.414 g cm⁻³ for *rac*-**BAmCl** and (*R*)-**BAmCl**, respectively. This result obeys the empirical Wallach's rule which states that racemic crystals tend to be denser than those of the corresponding enantiomeric crystals[7,11]. The crystalline structures were drastically changed after the chiral resolution.

Next, the luminescent properties of *rac*-**BAmCl** and (*R*)-**BAmCl** were evaluated (Fig. 2). As shown in Table 1, the absolute quantum efficiencies Φ_Fs of both crystalline samples recorded were much higher than those in solution and amorphous (prepared by a melt quenching method), clearly indicating that **BAmCl** possesses significant CIE properties. According to our previous report, it was proposed that the excited energy in the dilute solution state was deactivated by large structural relaxation in the excited state, while in the crystalline state, intermolecular interactions restrict molecular motions.[4a] In addition, the efficient packings and ordered molecular arrangement in crystalline states drastically changed the electronic states of single molecules via electronic intermolecular interactions, which led to enhanced Φ_F value. Similarly to this mechanism, emission enhancement should be induced by suppression of molecular motions and subsequently enhanced electronic intermolecular interactions in crystals.[4a]

To gather deep insight on the relationship between crystalline structures and photophysical properties, we determined kinetic parameters including radiative (k_r) and non-radiative rate constants (k_{nr}), which represent the sum of rates in each process with or without emission, respectively (Fig. S14). From the

comparison of calculated values, the k_rs of both crystalline samples were detected in the same range (10⁸ s⁻¹), whereas the k_{nr} value of (*R*)-**BAmCl** was one order higher than that of *rac*-**BAmCl**. Loose packing in crystal often allows molecular tumbling followed by acceleration of non-radiative decay processes.[12] Due to the lower density of the (*R*)-**BAmCl** crystal, it is likely that intramolecular motions could occur in the excited state, and non-radiative decay should be facilitated. The very small Φ_F and large k_{nr} values in solution can support this mechanism. Further, in comparison to (*R*)-**BAmCl**, slight reduction of k_r and red shift of the emission band were observed from *rac*-**BAmCl**. These results can be explained by the tight packing. Electronic states can be stabilized by intermolecular interactions in condensed states, whereas concentration quenching should be simultaneously caused. Therefore, the emission band with shorter lifetime in the longer wavelength region could be obtained from *rac*-**BAmCl**. In summary, it can be said that **BAmCl** basically has crystalline-state luminescent property. Owing to the unique molecular structure, intermolecular interactions, which tend to induce concentration quenching, can be disturbed, and intense emission can be obtained even in crystal. Furthermore, the luminescent properties including emission intensity and color are sensitive in the degree of molecular tumbling and molecular arrangements. As a consequence, not only CIE but also emission peak shifts are obtained.

Additionally, circularly polarized luminescence (CPL) properties were also examined. In solution, we were not able to obtain mirror imaging spectra because **BAmCl** enantiomers were intrinsically non-fluorescent in the solution states (Fig. S19). In solid, obvious mirror image CPL signals were detected in the emission region (Fig. S20). However, CPL intensity and dissymmetry factor, $g_{lum} = 2(I_{left} - I_{right})/ (I_{left} + I_{right})$ (I_{left}, I_{right}: PL intensities of left and right-handed CPL, respectively) were very low. Before solid-state CPL measurements, the crystal samples were highly compressed to form KBr tablets and critical decrease in crystallinities was induced. This treatment might decrease sensitivity for detecting the chiroptical properties of **BAmCl** in the solid states.

The thermogravimetric analysis (TGA) was conducted under N₂ atmosphere to compare thermal stability of the racemic and chiral crystals (Fig. S15 and S16). The initial decomposition temperature (T_i) of (*R*)-**BAmCl** (155 °C) was much lower than that of *rac*-**BAmCl** (227 °C). It is likely that molecular motions can vigorously occur by heating because of lower density packing in the crystal of (*R*)-**BAmCl**, and pyrolysis should proceed. Next, to investigate phase transition processes in solid, differential scanning calorimetry (DSC) measurements were performed (Fig. S17). In both crystals, the clear endothermic peaks attributed to the melting points were observed in the heating processes ($T_{m,onset}$ = 174 °C for *rac*-**BAmCl**; $T_{m,onset}$ = 139 °C for (*R*)-**BAmCl**). From the crystalline material involving a boron chirality center, it was reported that racemization can occur via the N–B bond dissociation.[13] Therefore, we also examined influence on the chirality with the (*R*)-**BAmCl** crystal by melting (Fig. S18). Accordingly, when the crystalline sample was heated at 120 °C, which is below T_m, for 20 min, the single
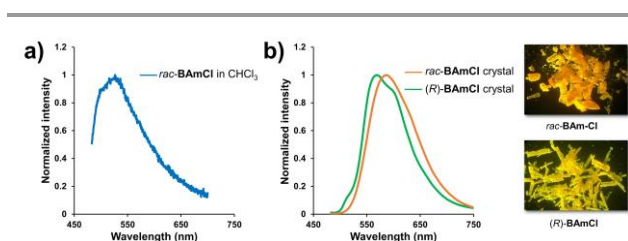

Fig. 2 Photoluminescence spectra of a) 1.0×10⁻⁵ M chloroform solution and b) crystalline states of *rac*-**BAmCl** and (*R*)-**BAmCl**. Picture images were obtained under UV irradiation (λ_{ex} = 365 nm, right).

peak corresponded to (*R*)-**BAmCl** was detected in the chiral HPLC profile, meaning that racemization hardly occurred. In contrast, after heating at 150 °C for 20 min, the molten sample was obtained, and the additional broad peak corresponding to the (*S*)-enantiomer was detected with the slight shoulder caused by pyrolysis. Surprisingly, according to the peak integral ratios, it was shown that both enantiomers exist with almost same proportions (I_R/I_S = 1.02, *I*: Integration of peak area for each enantiomer). This result clearly indicates that racemization completely proceeded at the molten liquid state.[14] To the best our knowledge, this is the first example to induce racemization at the boron stereogenic center in solid without any solvents. This multi temperature-responsive ability based on chiroptical information and luminescent signal change would be applicable for extensive usages, such as chiroptical sensing, optical displays and information storage.

In conclusion, we demonstrate in this research that chiral resolution of flexible fused-skeleton having a stereogenic boron center should be a valid strategy for creating luminescent polymorphic materials. The structural analyses for racemic crystal *rac*-**BAmCl** and homochiral crystal (*R*)-**BAmCl** reveal that their molecular arrangements are totally different: the molecules in *rac*-**BAmCl** formed dense dimeric structures between the (*R*)- and (*S*)-enantiomers, whereas (*R*)-enantiomers in (*R*)-**BAmCl** loosely stacked in helical-shaped molecular motifs. These structural differences have a significant influence on the crystalline-state emissive properties and these crystals displayed distinct different emission colors. Interestingly, the heat-initiated homogeneous racemization without any solvents and catalysts was observed in the molten state of crystal (*R*)-**BAmCl**. This dynamic stereochemical behavior in homogenous media would be a promising scaffold for constructing the solid-state stimuli-responsive materials.

Conflicts of interest

There are no conflicts to declare.

Notes and references

1   (a) Y. Liu, K.-R. Wang, D.-S. Guo and B.-P. Jiang, *Adv. Funct. Mater.*, 2009, **19**, 2230–2235. (b) S. Saotome, K. Suenaga, K. Tanaka and Y. Chujo, *Mater. Chem. Front.*, 2020, **4**, 1781–1788. (c) K. Li, Y. Chen, W. Lu, N. Zhu and C.-M. Che, *Chem. – Eur. J.*, 2011, **17**, 4109–4112.

2   (a) S.-W. Zhang and T. M. Swager, *J. Am. Chem. Soc.*, 2003, **125**, 3420–3421; (b) L. Basabe-Desmonts, D. N. Reinhoudt and M. Crego-Calama, *Chem. Soc. Rev.*, 2007, **36**, 993–1017.

3   (a) Y. Chujo and K. Tanaka, *Bull. Chem. Soc. Jpn.*, 2015, **88**, 633–643; (b) M. Gon, K. Tanaka and Y. Chujo, *Polym. J.*, 2017, **50**, 109–126; (c) K. Tanaka and Y. Chujo, *Polym. J.*, 2020, **52**, 555–566; (d) M. Gon, K. Tanaka and Y. Chujo, *Bull. Chem. Soc. Jpn.*, 2019, **92**, 7–18.

4   (a) S. Ohtani, M. Gon, K. Tanaka and Y. Chujo, *Chem. – Eur. J.*, 2017, **23**, 11827–11833; (b) S. Ohtani, M. Gon, K. Tanaka and Y. Chujo, *Macromolecules*, 2019, **52**, 3387–3393; (c) S. Ohtani, M. Nakamura, M. Gon, K. Tanaka and Y. Chujo, *Chem. Commun.*, 2020, **56**, 6575–6578; (d) S. Ohtani, M. Gon, K. Tanaka and Y. Chujo, *Crystals* 2020, **10**, 615.

5   (a) Y. Dong, J. W. Y. Lam, A. Qin, Z. Li, J. Sun, H. H.-Y. Sung, I. D. Williams and B. Z. Tang, *Chem. Commun.*, 2007, 40–42; (b) P. Galer, R. C. Korošec, M. Vidmar and B. Šket, *J. Am. Chem. Soc.*, 2014, **136**, 7383–7394. (c) T. Han, X. Feng, D. Chen and Y. Dong, *J. Mater. Chem. C*, 2015, **3**, 7446–7454.

6   (a) D. Gentili, M. Gazzano, M. Melucci, D. Jones and M. Cavallini, *Chem. Soc. Rev.*, 2019, **48**, 2502–2517. (b) Z. He, L. Zhang, J. Mei, T. Zhang, J. W. Y. Lam, Z. Shuai, Y. Q. Dong and B. Z. Tang, *Chem. Mater.*, 2015, **27**, 6601–6607. (c) G. Zhang, J. Lu, M. Sabat and C. L. Fraser, *J. Am. Chem. Soc.*, 2010, **132**, 2160–2162. (d) X. Gu, J. Yao, G. Zhang, Y. Yan, C. Zhang, Q. Peng, Q. Liao, Y. Wu, Z. Xu, Y. Zhao, H. Fu and D. Zhang, *Adv. Funct. Mater.*, 2012, **22**, 4862–4872.

7   (a) O. Wallach *Justus Liebigs Ann. Chem.*, 1895, **286**, 90–143; (b) T. Friščić, L. Fábián, J. C. Burley, D. G. Reid, M. J. Duer and W. Jones, *Chem. Commun.*, 2008, 1644–1646.

8   (a) A. Wakamiya, T. Taniguchi and S. Yamaguchi, *Angew. Chem. Int. Ed.*, 2006, **45**, 3170–3173; (b) Y. Adachi, Y. Ooyama, Y. Ren, X. Yin, F. Jäkle and J. Ohshita, *Polym. Chem.*, 2018, **9**, 291–299; (c) M. Hesari, S. M. Barbon, V. N. Staroverov, Z. Ding and J. B. Gilroy, *Chem. Commun.*, 2015, **51**, 3766–3769; (d) J. Yoshino, N. Kano and T. Kawashima, *J. Org. Chem.*, 2009, **74**, 7496–7503; (e) A. Sundararaman, M. Victor, R. Varughese and F. Jäkle, *J. Am. Chem. Soc.*, 2005, **127**, 13748–13749; (f) M. Urban, K. Durka, P. Jankowski, J. Serwatowski and S. Luliński, *J. Org. Chem.*, 2017, **82**, 8234–8241.

9   (a) A. Haefele, C. Zedde, P. Retailleau, G. Ulrich and R. Ziessel, *Org. Lett.*, 2010, **12**, 1672–1675; (b) V. G. Jiménez, F. M. F. Santos, S. Castro-Fernández, J. M. Cuerva, P. M. P. Gois, U. Pischel and A. G. Campaña, *J. Org. Chem.*, 2018, **83**, 14057–14062.

10   S. Varughese, *J. Mater. Chem. C*, 2014, **2**, 3499–3516.

11   M. Jin, T. Seki and H. Ito, *Chem. Commun.*, 2016, **52**, 8083–8086.

12   (a) Y. Akune, R. Hirosawa, N. Endo, S. Hatano, T. Hosokai, H. Sato and S. Matsumoto, *CrystEngComm*, 2017, **19**, 1947–1952. (b) T. Hinoue, Y. Mizobe, I. Hisaki, M. Miyata and N. Tohnai, *Chem. Lett.*, 2008, **37**, 642–643. (c) I. Hisaki, E. Kometani, H. Shigemitsu, A. Saeki, S. Seki, N. Tohnai and M. Miyata, *Cryst. Growth & Des.*, 2011, **11**, 5488–5497.

13   (a) M. Oki and M. Ohira, *Bull. Chem. Soc. Jpn.*, 1984, **57**, 3117–3121; (b) S. Toyota, T. Hakamata, N. Nitta and F. Ito, *Chem. Lett.*, 2004, **33**, 206–207; (c) S. Schlecht, W. Frank and M. Braun, *Beilstein J. Org. Chem.*, 2011, **7**, 615–621.

14   H. Wu and A. West, *Crystal Growth & Design*, 2011, **11**, 3366–3374.

京都大学
KYOTO UNIVERSITY

Supporting Information

Facile Strategy for Obtaining Luminescent Polymorphs Based on Chirality of Boron-Fused Azomethine Complex

Shunsuke Ohtani, Yusuke Takeda, Masayuki Gon, Kazuo Tanaka* and Yoshiki Chujo

Department of Polymer Chemistry, Graduate School of Engineering, Kyoto University Katsura, Nishikyo-ku, Kyoto 615-8510, Japan

E-mail: tanaka@poly.synchem.kyoto-u.ac.jp

General

^{1}H (400 MHz), ^{13}C (100 MHz) ^{11}B (128 MHz) NMR spectra were recorded on JEOL JNM-AL400 or JNM-EX400 spectrometers. Samples were analyzed in CDCl$_3$ and DMSO-d$_6$. The chemical shift values were expressed relative to tetramethylsilane (TMS) for ^{1}H and ^{13}C NMR as an internal standard in CDCl$_3$ and BF$_3$·OEt$_2$ for ^{11}B NMR as a capillary standard. Analytical thin-layer chromatography (TLC) was performed with silica gel 60 Merck F254 plates. Column chromatography was performed with Wakogel® C-300 silica gel. High-resolution mass (HRMS) spectrometry was performed at the Technical Support Office (Department of Synthetic Chemistry and Biological Chemistry, Graduate School of Engineering, Kyoto University), and the HRMS spectra were obtained on a Thermo Fisher Scientific EXACTIVE spectrometer for electrospray ionization (ESI). UV–vis–NIR absorption spectra were recorded on a SHIMADZU UV-3600 spectrophotometer, and samples were analyzed at room temperature. Photoluminescence (PL) spectra were measured on a HORIBA JOBIN YVON Fluoromax-4P spectrofluorometer. Absolute PL quantum efficiency was measured on a Hamamatsu Photonics Quantaurus-QY Plus C13534-01. The PL lifetime measurement was performed on a Horiba FluoroCube spectrofluorometer system; excitation was carried out using a UV diode laser (NanoLED 375 nm). X-ray crystallographic analysis was carried out by Rigaku R-AXIS RAPID-F imaging plate diffractometer with graphite-monochromated MoKα radiation and Rigaku Saturn 724+ with MicroMax-007HF CCD diffractometer with Varimax Mo optics using graphite-monochromated MoKα radiation. The analysis was carried out with direct methods (SHELX-2014/7) using Yadokari-XG. The program Mercury 3.3.1 was used to generate the X-ray structural diagram. Thermogravimetric analyses (TGA) were recorded on a Hitachi High-Tech Science Corp. STA7200RV. Differential scanning calorimetry (DSC) was recorded on a Hitachi High-Tech Science Corp. DSC7020. Circular dichroism (CD) spectra were measured on a JASCO J-820 spectropolarimeter. Circularly polarized luminescence (CPL) spectra were recorded on a JASCO CPL-200S spectrofluoropolarimeter. Solid-state CPL spectra were measured for (*R*)- and (*S*)-**BAmCl** (0.5 mg) mixed with KBr (150 mg). Tablets (diameter: 10 mm, (*R*)- or (*S*)-**BAmCl**/KBr) were prepared using a tablet forming machine (48.2 kN, press time: 3 min). Chiral high performance liquid chromatography (HPLC) was performed with YMC CHIRAL ART Amylose-SA (5μm) 250×20 mml.D. and SHIMADZU Prominence Modular HPLC system. Specific rotations ([α]^t_D) were measured with a Rudolph Research AUTOPOL IV Automatic Polarimeter.

Materials

Commercially available compounds used without purification:

2-Amino-5-chlorophenol (Tokyo Chemical Industry Co, Ltd.)

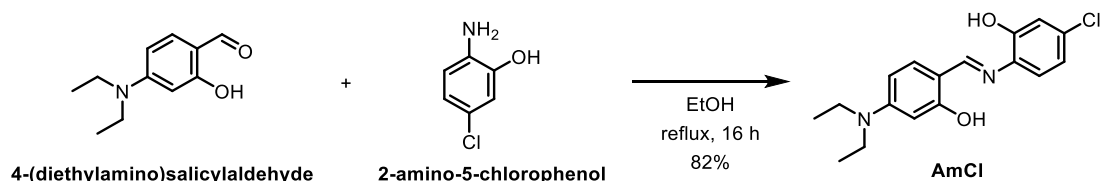4-(Diethylamino)salicylaldehyde (Tokyo Chemical Industry Co, Ltd.)

Boron trifluoride diethyl etherate ($\geq$46% BF_3 basis) ($BF_3 \cdot OEt_2$) (Sigma-Aldrich Co. LLC.)

Commercially available solvents:

EtOH (Wako Pure Chemical Industries, Ltd.), $CHCl_3$ (Wako Pure Chemical Industries, Ltd.), n-hexane (Wako Pure Chemical Industries, Ltd.) and CH_2Cl_2 (Wako Pure Chemical Industries, Ltd.) were used without further purification. Deoxidized grade toluene (Wako Pure Chemical Industries, Ltd.) were used without further purification. Triethylamine (Kanto Chemical Co., Inc.) was purified by passage through solvent purification columns under argon pressure.

Synthetic Procedures and Characterization

Synthesis of AmCl

Scheme S1. Synthesis of **AmCl**.

2-Amino-5-chlorophenol (0.37 g, 2.59 mmol) was dissolved in 20 mL of EtOH. 4-(Diethylamino)salicylaldehyde (0.50 g, 2.59 mmol) was added to the solution and the reaction mixture was stirred at reflux temperature for 16 h. During course of the reaction, the product was precipitated from the reaction mixture. After cooling to room temperature, the resulting mixture was poured into water. The precipitation collected by filtration was dried *in vacuo* to give **AmCl** as an orange solid (0.68 g, 82%). ^{1}H NMR (CDCl$_3$, 400 MHz), δ (ppm): 8.40 (s, 1H), 7.19 (d, J = 8.8 Hz, 1H), 7.00−6.98 (m, 2H), 6.89 (dd, J = 8.3, 2.2 Hz, 1H), 6.28 (dd, J = 8.8, 2.4 Hz, 1H), 6.19 (d, J = 2.4 Hz, 1H), 3.42 (q, J = 7.1 Hz, 4H), 1.22 (t, J = 7.1 Hz, 6H). ^{13}C NMR (DMSO-d$_6$, 100 MHz), δ (ppm): 164.5, 159.8, 151.6, 151.2, 134.6, 133.9, 129.4, 119.9, 119.3, 115.8, 108.9, 103.7, 97.0, 43.8, 12.5. HRMS (ESI): Calcd for [M+H]$^+$, 319.1208; Found, m/z 319.1203. Elemental analysis calcd. for C$_{17}$H$_{19}$ClN$_2$O$_2$: C, 64.05; H, 6.01; N, 8.79. Found: C, 64.10; H, 5.91; N, 8.89.
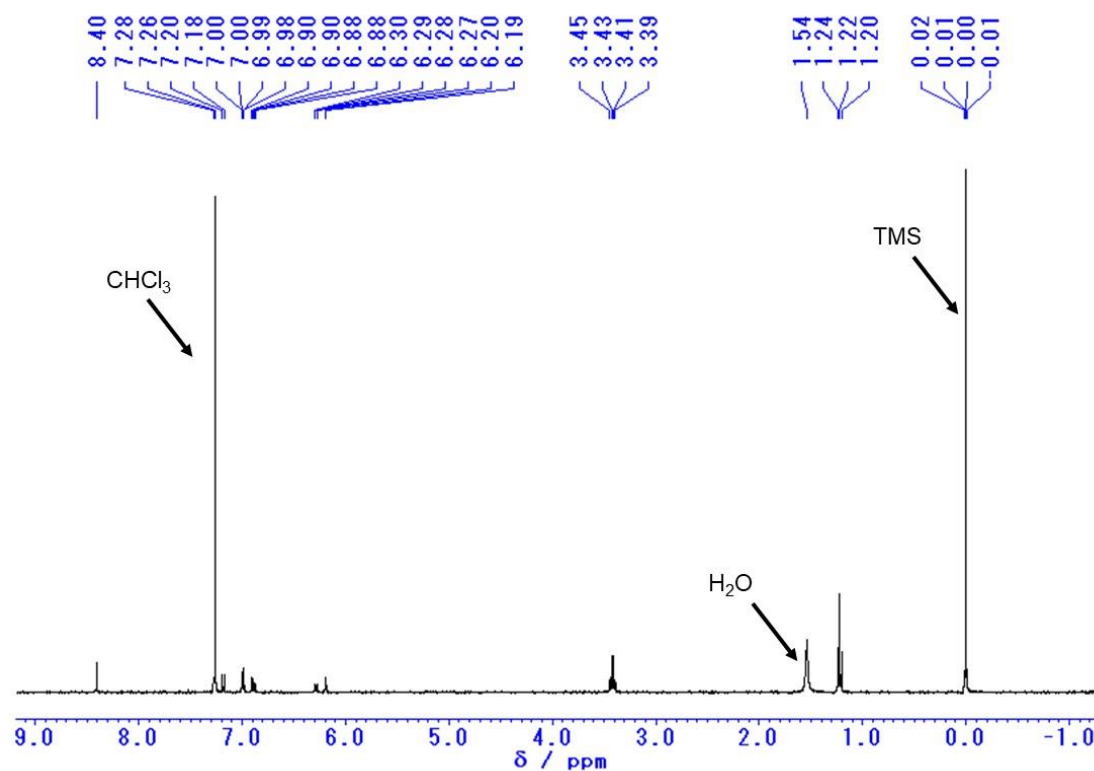
Fig. S1. ^{1}H NMR spectrum of **AmCl**, CDCl$_3$, 400 MHz.
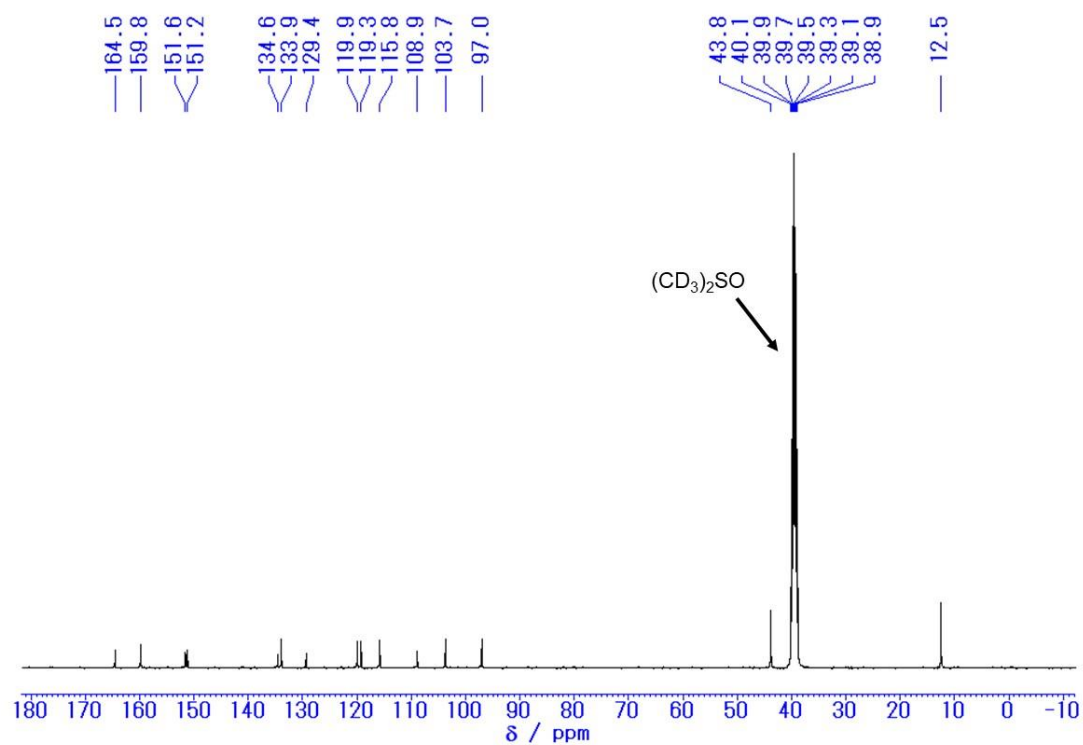
Fig. S2. ^{13}C NMR spectrum of **AmCl**, DMSO-d$_6$, 100 MHz.

Synthesis of BAmCl
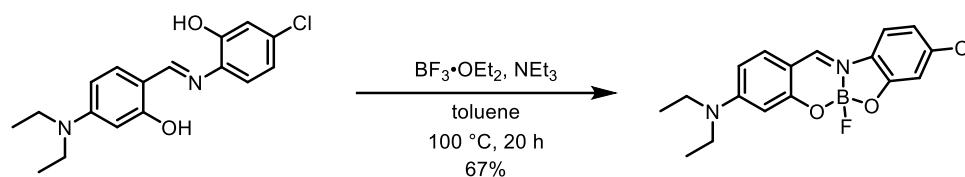
Scheme S2. Synthesis of **BAmCl**.

Am-Cl (0.40 g, 1.25 mmol) was dissolved in 13 mL of dry toluene under Ar atmosphere at room temperature and triethylamine (4 mL) was then added to the solution. $BF_3 \cdot OEt_2$ (3 mL) was added dropwise to the solution and the reaction mixture was stirred at 100 °C for 20 h. After cooling to room temperature, the resulting mixture was quenched by EtOH and concentrated by a rotary evaporator. The residue was purified by chromatography on silica gel with CH_2Cl_2 and dissolved in small amount of $CHCl_3$, and the product was reprecipitated from hexane to give **BAmCl** as an orange solid (0.29 g, 67%). $R_f = 0.79$ (CH_2Cl_2). HRMS (ESI): Calcd for $[M+Na]^+$, 347.1128; Found, m/z 347.1121. Elemental analysis calcd. for $C_{17}H_{17}BClFN_2O_2$: C, 58.91; H, 4.94; N, 8.08. Found: C, 58.84; H, 4.94; N, 8.07.

Racemic **BAmCl**:

^{1}H NMR (CDCl$_3$, 400 MHz), δ (ppm): 8.25 (s, 1H), 7.31 (d, J = 9.3 Hz, 1H), 7.22 (d, J = 8.3 Hz, 1H), 7.06 (d, J = 2.0 Hz,1H), 6.86 (dd, J = 8.4, 2.0 Hz, 1H), 6.43 (dd, J = 9.1, 2.5 Hz, 1H), 6.37 (d, J = 2.4 Hz, 1H), 3.47 (m, 4H), 1.25 (t, J = 7.1 Hz, 6H). ^{11}B NMR (CDCl$_3$, 128 MHz), δ (ppm): 4.27 (d, J = 38 MHz). ^{13}C NMR (CDCl$_3$, 100 MHz), δ (ppm): 160.1, 156.4, 155.9, 148.1, 133.8, 133.4, 129.5, 119.4, 114.7, 113.4, 108.6, 107.4, 99.5, 45.2, 12.7.

Enantiomeric **BAmCl-fr1** ((*R*)-**BAmCl**):

$[\alpha]^{23}_D$ = +1226.5 (*c* 0.1, CHCl$_3$)

^{1}H NMR (CDCl$_3$, 400 MHz), δ (ppm): 8.25 (s, 1H), 7.31 (d, J = 9.0 Hz, 1H), 7.22 (d, J = 8.3 Hz, 1H), 7.06 (d, J = 1.9 Hz, 1H), 6.87 (dd, J = 8.6, 2.2 Hz, 1H), 6.44 (dd, J = 9.0, 2.4 Hz, 1H), 6.37 (d, J = 2.4 Hz, 1H), 3.47 (m, 4H), 1.25 (t, J = 7.1 Hz, 6H). ^{11}B NMR (CDCl$_3$, 128 MHz), δ (ppm): 4.27 (d, J = 38 MHz). ^{13}C NMR (CDCl$_3$, 100 MHz), δ (ppm): 160.1, 156.4, 155.9, 148.0, 133.9, 133.4, 129.5, 119.4, 114.7, 113.4, 108.7, 107.4, 99.6, 45.2, 12.7.

Enantiomeric **BAmCl-fr2** ((*S*)-**BAmCl**):

$[\alpha]^{23}_D$ = −1244.6 (*c* 0.1, CHCl$_3$)

The NMR spectra of **BAmCl-fr2** were the same with **BAmCl-fr1**.
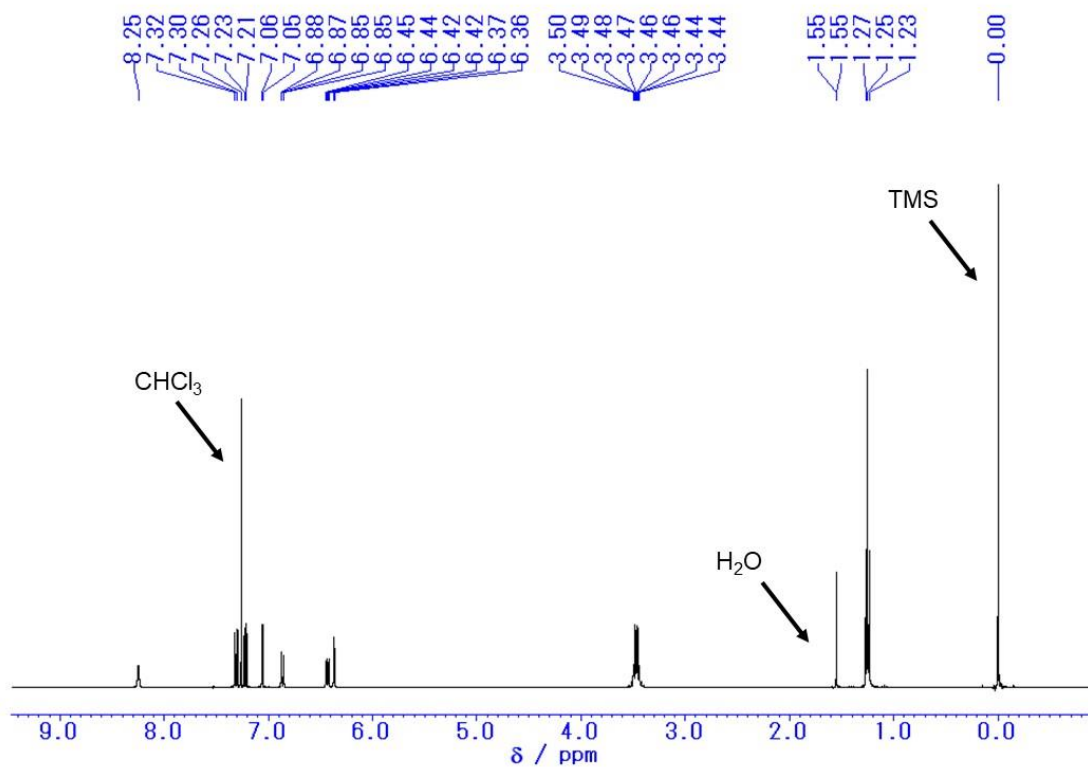
Fig. S3. ^{1}H NMR spectrum of racemic **BAmCl**, CDCl$_3$, 400 MHz.
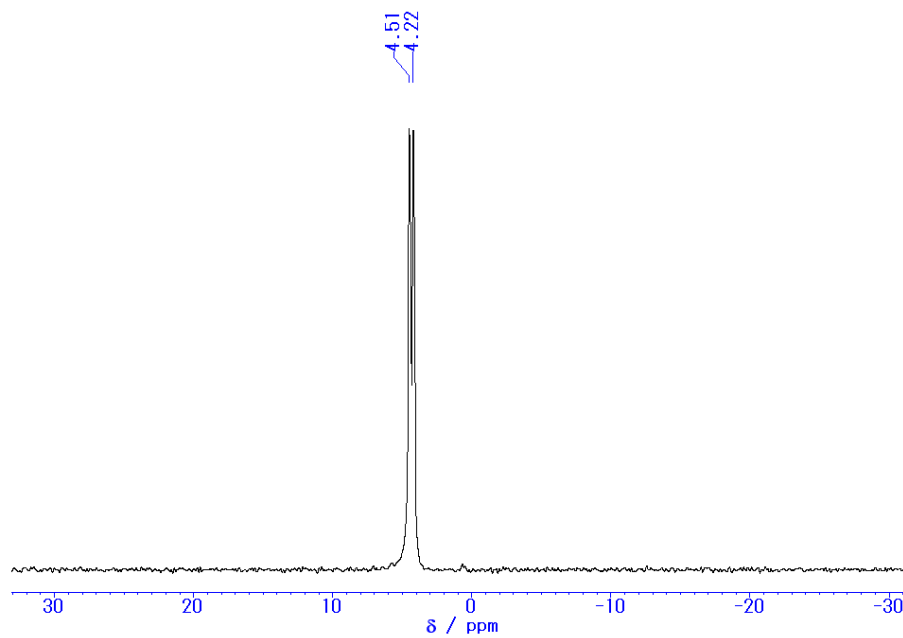
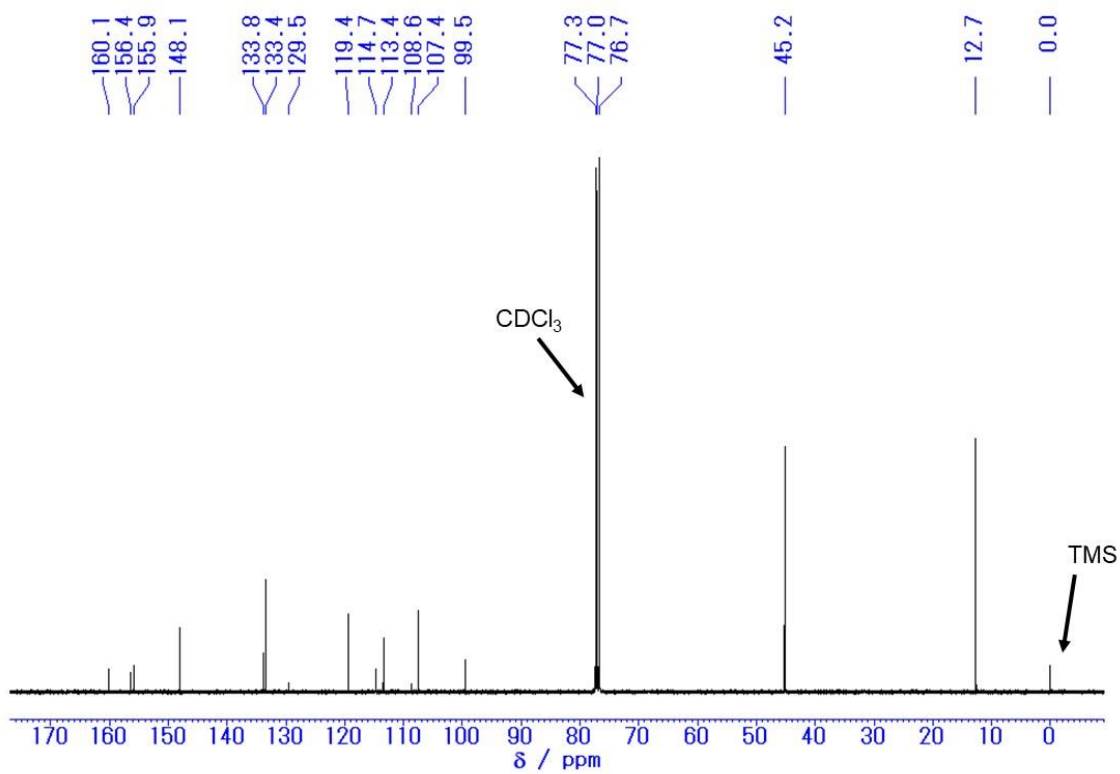**Fig. S4.** ^{11}B NMR spectrum of racemic **BAmCl**, CDCl$_3$, 128 MHz.

Fig. S5. ^{13}C NMR spectrum of racemic **BAmCl**, CDCl$_3$, 100 MHz.
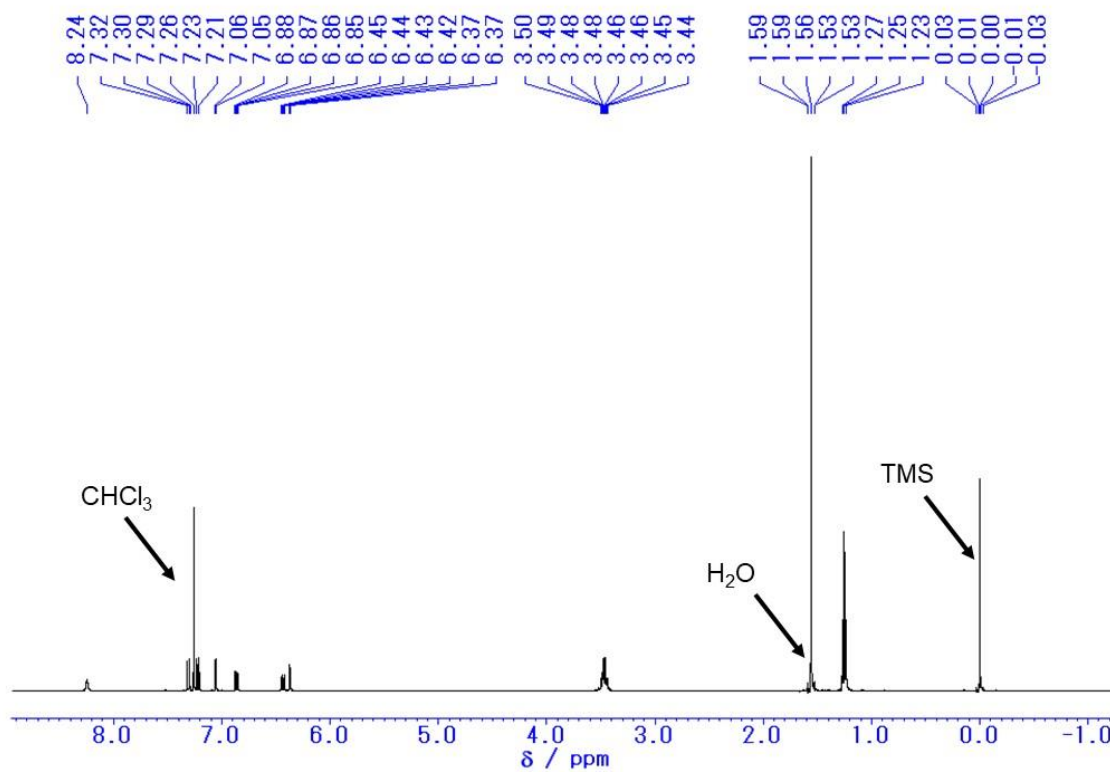
Fig. S6. ^{1}H NMR spectrum of enantiomeric **BAmCl-fr1 ((*R*)-BAmCl)**, CDCl$_3$, 400 MHz.
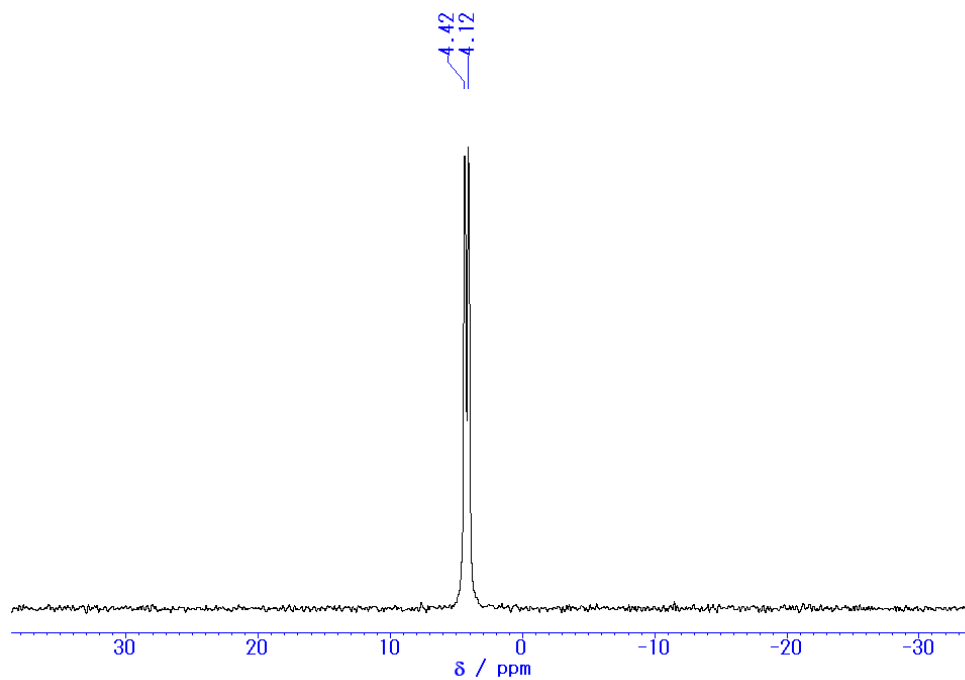

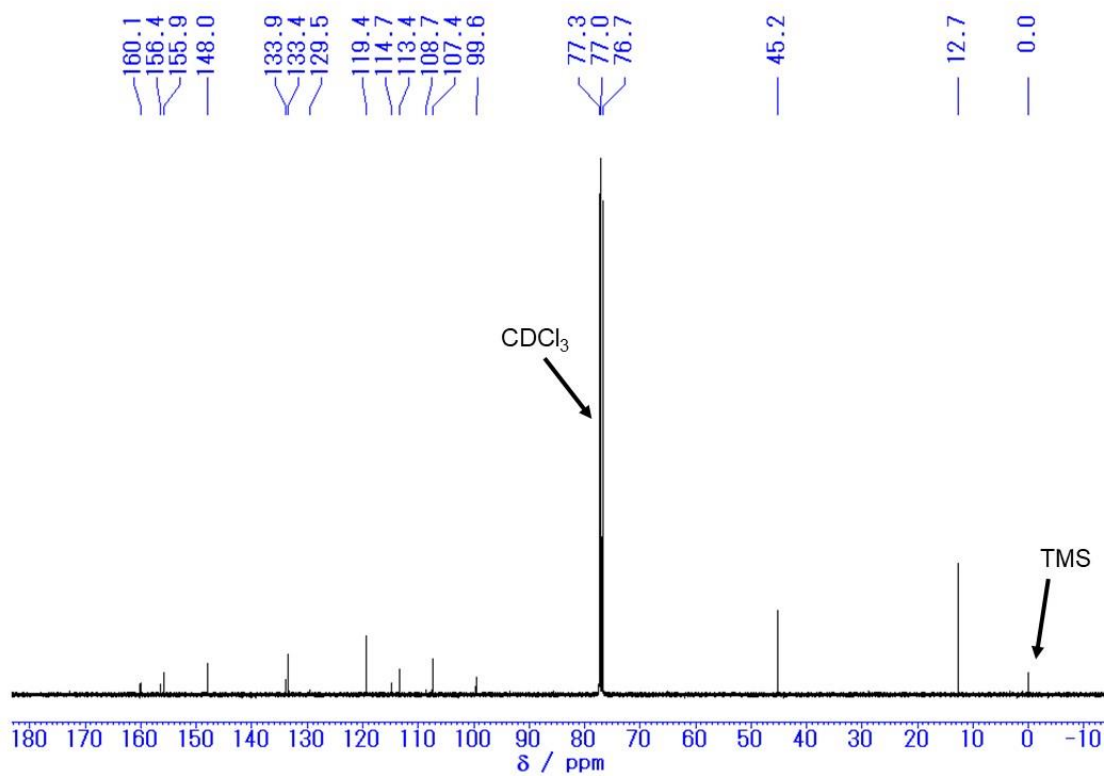**Fig. S7.** ^{11}B NMR spectrum of enantiomeric **BAmCl-fr1 ((*R*)-BAmCl)**, CDCl$_3$, 128 MHz.

Fig. S8. ^{13}C NMR spectrum of enantiomeric **BAmCl-fr1** ((*R*)-**BAmCl**), CDCl$_3$, 100 MHz.

Chiral resolution of racemate BAmCl

Table S1. Analysis condition of resolution by chiral HPLC

Column	YMC CHIRAL ART Amylose-SA (5 μm) 250 × 20 mml.D.
Eluent	*n*-hexane/THF (v/v = 1/3)
Flow rate	3.5 mL/min
Detection	UV at 250 nm
Injection	3.0 mL (6.7 mg/mL)
Retention Time	(*R*)-**BAmCl**: 57.2 min. (*S*)-**BAmCl**: 62.6 min.
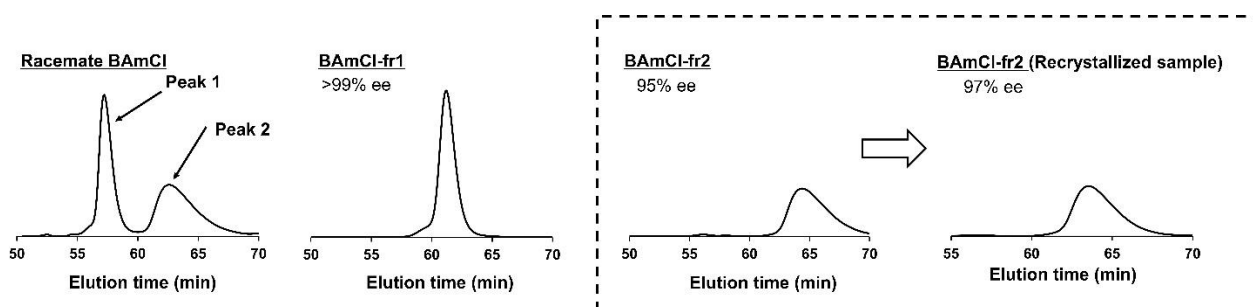
Fig. S9. Chiral HPLC profiles (*n*-hexane/THF 1/3 (v/v), UV/vis absorption detection at 250 nm) of compound **BAmCl**.

Circular dichroism (CD) study
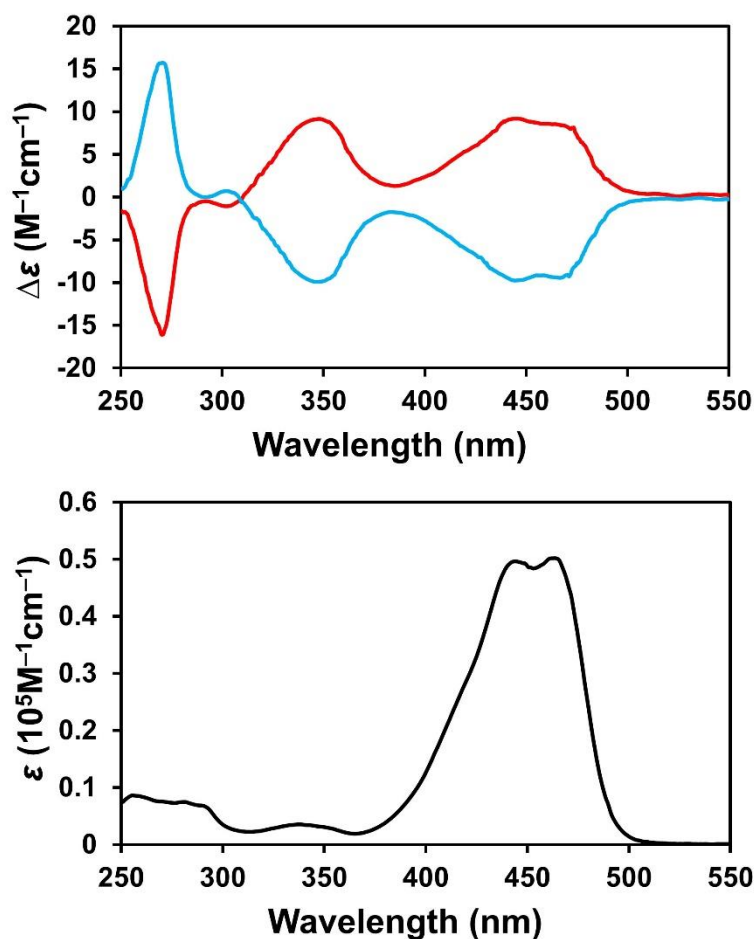
Fig. S10. Circular dichroism (CD) and UV–vis absorption spectra of 2.0×10^{-5} M chloroform solutions containing **BAmCl-fr1** (red) and **BAmCl-fr2** (blue).

Time-dependent circular dichroism (CD) study
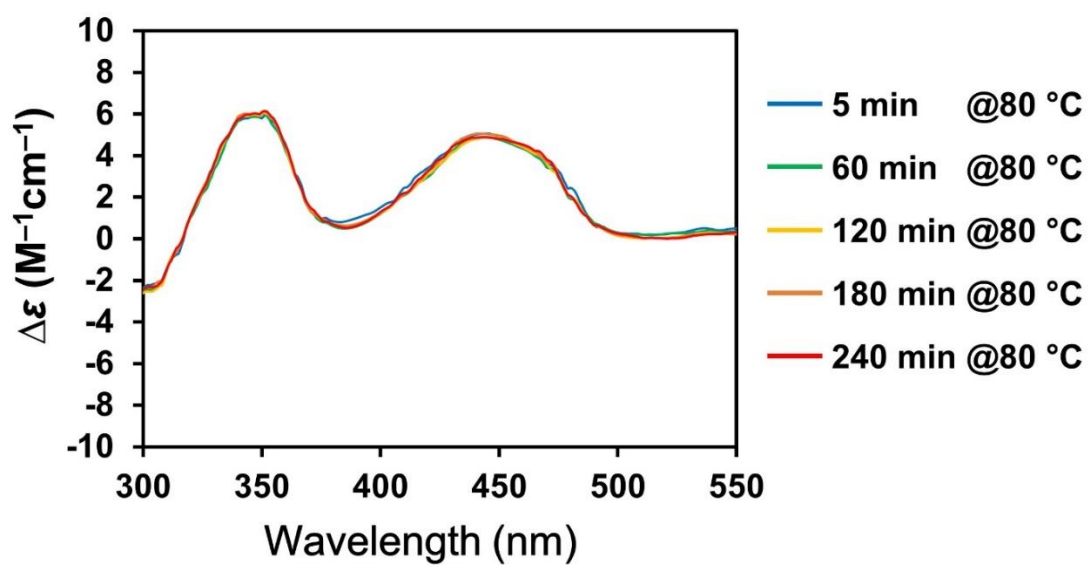
Fig. S11. Time-dependent circular dichroism (CD) spectra of **BAmCl-fr1** ((*R*)-**BAmCl**) in toluene solution (2.0×10^{-5} M) at 80 °C.

X-ray crystal structure analysis of *rac*-BAmCl

Intensity data were collected on a Rigaku R-AXIS RAPID imaging plate area detector with graphite monochromated MoKα radiation (λ = 0.71069 Å). The structures were solved and refined by full-matrix least-squares procedures based on F^2 (SHELXL-2014/7).

Single-crystal of *rac*-**BAmCl** was prepared by vapor diffusion method from CHCl₃ solution under hexane atmosphere at room temperature.

Table S2. Crystallographic data of *rac*-**BAmCl** at 78 K	
Morphology	Orange block
Space group	$P2_1/c$
a/Å	8.4212 (8)
b/Å	14.1413 (7)
c/Å	13.5406 (13)
α/deg	90
β/deg	101.611 (7)
γ/deg	90
V/Å³	1579.5 (3)
Z	4
Density/g cm⁻³	1.457
Absorption coefficient	0.265
F(000)	720
Crystal size (nm)	0.30 × 0.30 × 0.20
θ range for data collection	3.001–27.485
Limiting indices	$-10 \leq h \leq 10, -18 \leq k \leq 18, -17 \leq l \leq 17$
Reflections collected (unique)	14569/3118 [R(int) = 0.077]
Completeness to theta = 27.475	0.982
Goodness-off-fit on F^2	1.092
Final R indices [I > 2σ(I)][a]	R_1 = 0.0507 wR_2 = 0.1382
R indices (all data)	R_1 = 0.0577 wR_2 = 0.1432
T/K	78

[a] $R_1 = \Sigma(|F_0|-|F_c|)/\Sigma|F_0|$. w$R_2 = [\Sigma w(F^2_0 - F^2_c)2/ \Sigma w(F^2_0)^2]^{1/2}$. w = $1/[\sigma^2(F^2_0)+[(ap)^2 + bp]]$, where p = $[\max(F^2_0, 0) + 2F^2_c]/3$.
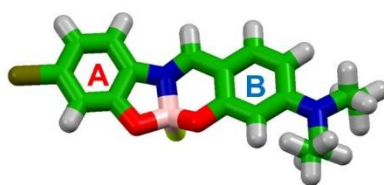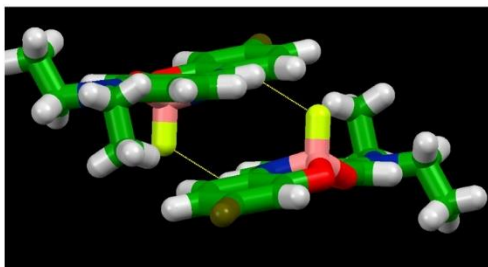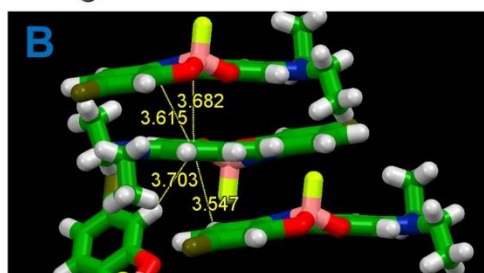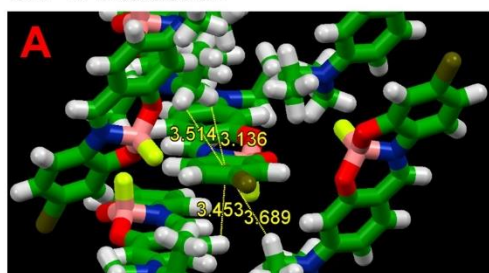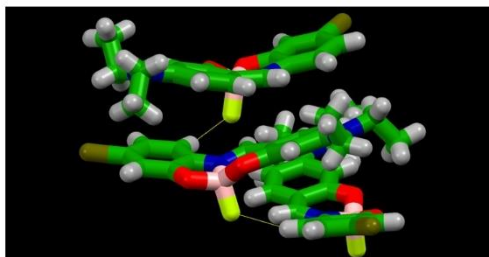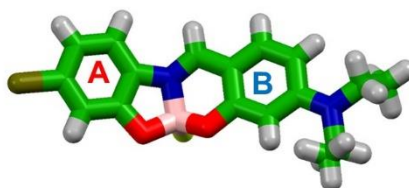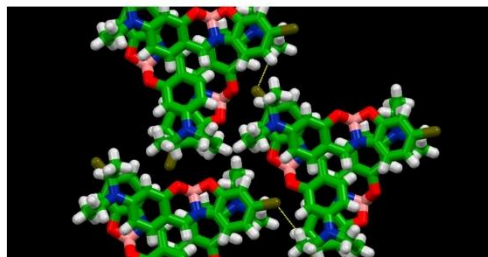
Fig. S12. Intermolecular interaction patterns of *rac*-**BAmCl**. a) CH···F interaction b) CH···π interaction between hydrogen atoms and aromatic rings A or B.

X-ray crystal structure analysis of (*R*)-BAmCl

Intensity data were collected on a Rigaku Saturn 724+ with MicroMax-007HF CCD diffractometer with Varimax Mo optics using graphite-monochromated MoKα radiation. The structures were solved and refined by full-matrix least-squares procedures based on F^2 (SHELXL-2014/7).

Single-crystal of (*R*)-**BAmCl** was prepared by vapor diffusion method from THF solution under hexane atmosphere at room temperature.

Table S3. Crystallographic data of (*R*)-**BAmCl** at 143 K	
Morphology	Orange needle
Space group	$P3_2$
a/Å	12.8397 (12)
b/Å	12.8397 (12)
c/Å	8.5551 (11)
α/deg	90
β/deg	90
γ/deg	120
V/Å³	1221.4 (3)
Z	3
Density/g cm⁻³	1.414
Absorption coefficient	0.257
F(000)	540
Crystal size (nm)	$0.360 \times 0.150 \times 0.100$
θ range for data collection	3.004–27.462
Limiting indices	$-15 \leq h \leq 16, -16 \leq k \leq 16, -10 \leq l \leq 11$
Reflections collected (unique)	219/3657 [R(int) = 0.0341]
Completeness to theta = 27.462	0.980
Goodness-off-fit on F^2	1.008
Final R indices [I > 2σ(I)][a]	$R_1 = 0.0342$ w$R_2 = 0.0853$
R indices (all data)	$R_1 = 0.0386$ w$R_2 = 0.0876$
T/K	143

[a] $R_1 = \Sigma(|F_0|-|F_c|)/\Sigma|F_0|$. w$R_2 = [\Sigma w(F^2{}_0-F^2{}_c)2/ \Sigma w(F^2{}_0)^2]^{1/2}$. w $= 1/[\sigma^2(F^2{}_0)+[(ap)^2+bp]]$, where p $= [\max(F^2{}_0,0)+2F^2{}_c]/3$.
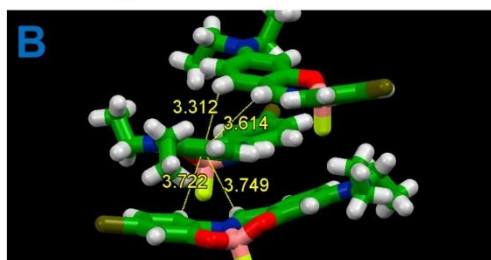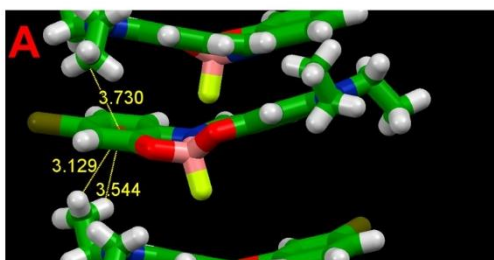
Fig. S13. Intermolecular interaction patterns of (*R*)-**BAmCl**. a) CH···F interaction b) CH···Cl interaction c) CH···π interaction between hydrogen atoms and aromatic rings A or B.
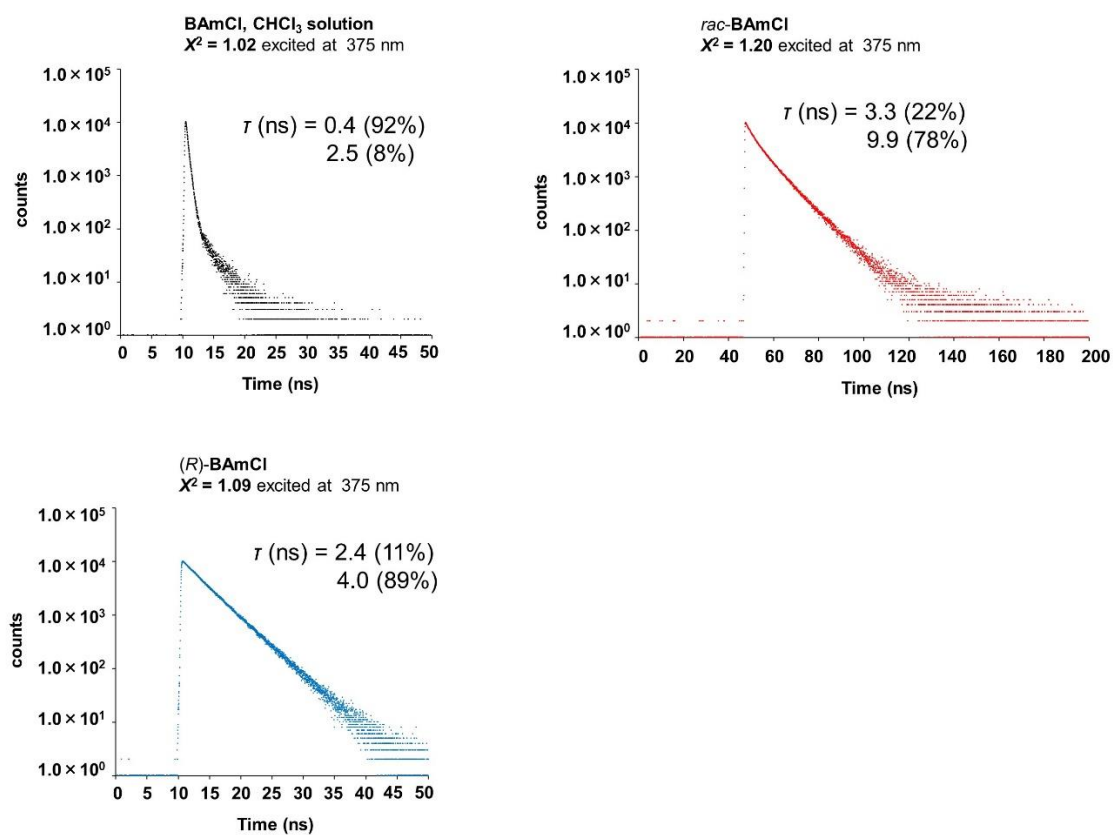
PL lifetime decay curves

Fig. S14. PL lifetime decay curves of **BAmCl** in chroloform solution (1.0×10^{-5} M) and crystalline states *rac*-**BAmCl** and (*R*)-**BAmCl** at room temperature. Their emissions at the PL peak tops were monitored.
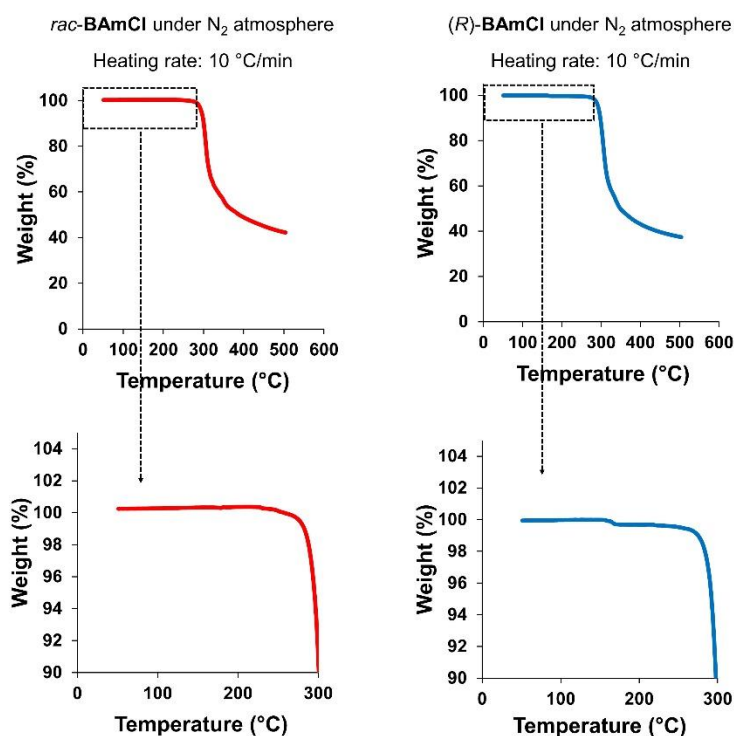
Thermogravimetric analysis (TGA)

Fig. S15. Thermogravimetric analyses (TGA) curves of *rac*-**BAmCl**, (*R*)-**BAmCl** and (*S*)-**BAmCl**.

We investigated about the initial mass loss in TGA curve of (*R*)-**BAmCl** by using ^{1}H NMR measurement (Figure S15). After heating at 180 °C for 20 min, (*R*)-**BAmCl** showed several peaks in aromatic region of ^{1}H NMR. Therefore, we concluded that the initial mass loss was not related to the sublimation or impurity, but to the decomposition of (*R*)-**BAmCl**.
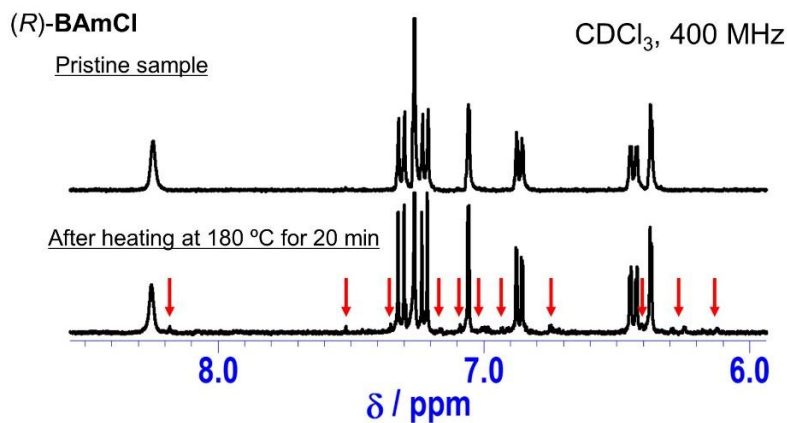
Fig. S16. ^{1}H NMR spectra of pristine and heated (*R*)-**BAmCl** crystalline sample.

Differential scanning calorimetric (DSC) analysis
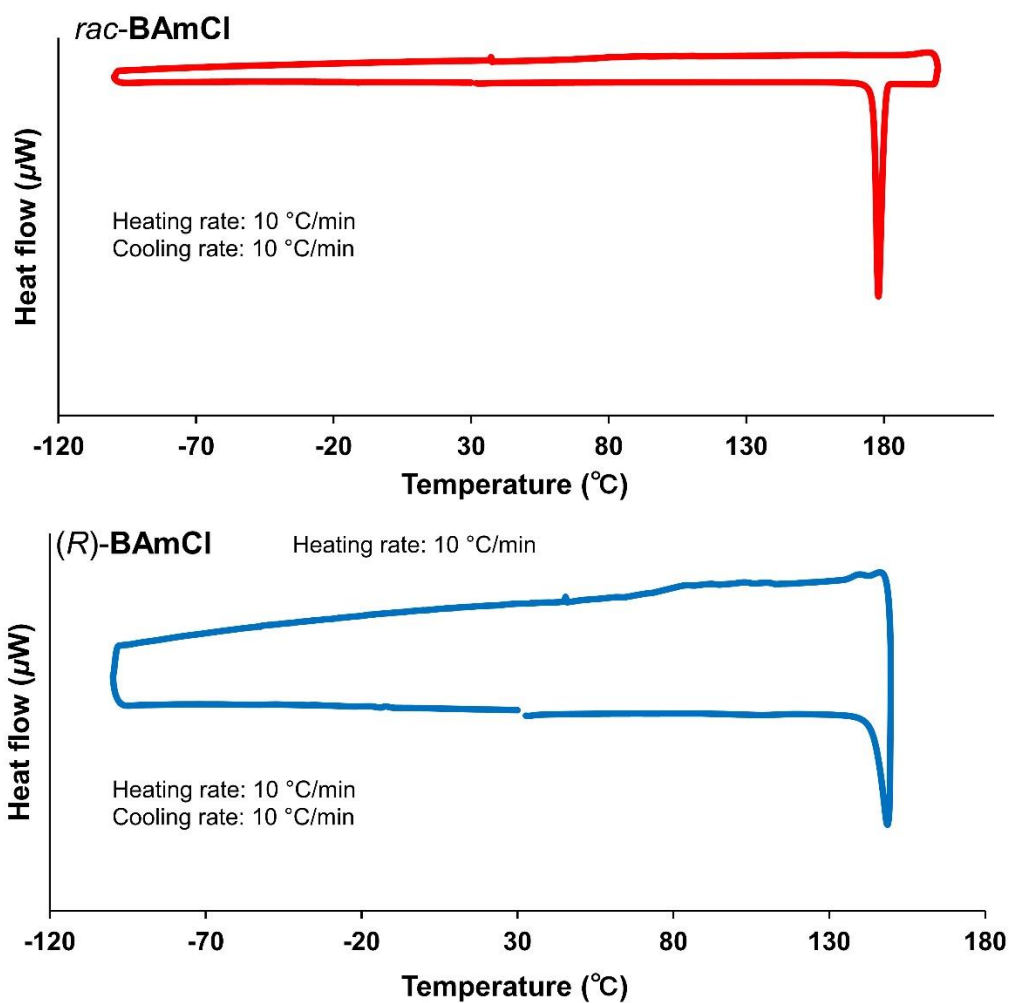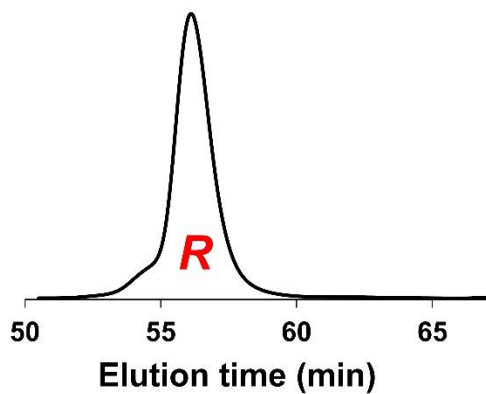

Fig. S17. Differential scanning calorimetric (DSC) curves of *rac*-**BAmCl** and (*R*)-**BAmCl**.

Racemization study of (*R*)-BAmCl

After heating at 120 °C for 20 min

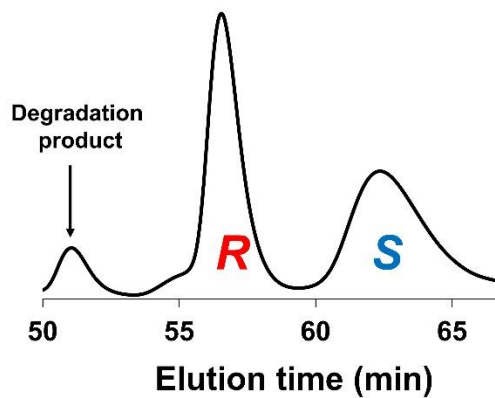**After heating at 150 °C for 20 min**

Fig. S18. Chiral HPLC chromatograms (*n*-hexane/THF 1/3 (v/v), UV/vis absorption detection at 250 nm) of crystalline sample (*R*)-**BAmCl**.
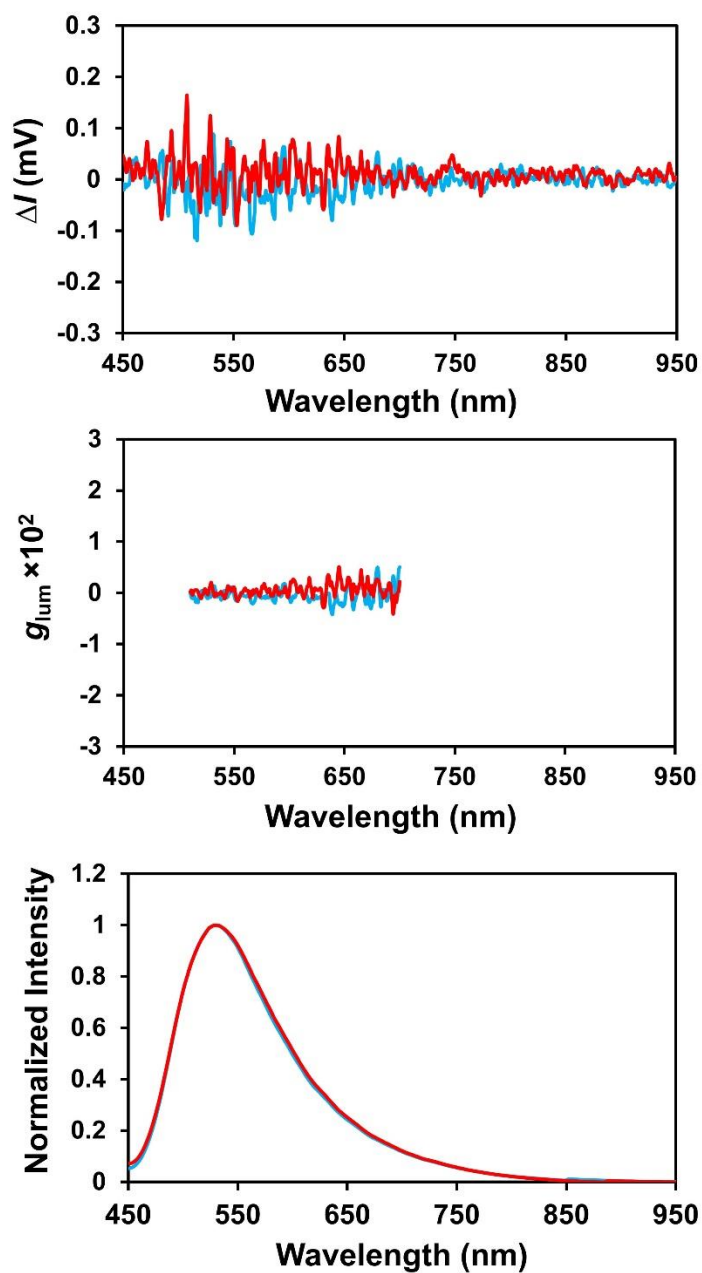
Fig. S19. CPL (top), g_{lum} (middle), and PL (bottom) spectra of (*R*)-**BAmCl** (red) and (*S*)-**BAmCl** (blue) CHCl$_3$ solution (1.0×10^{-4} M) excited at 350 nm.
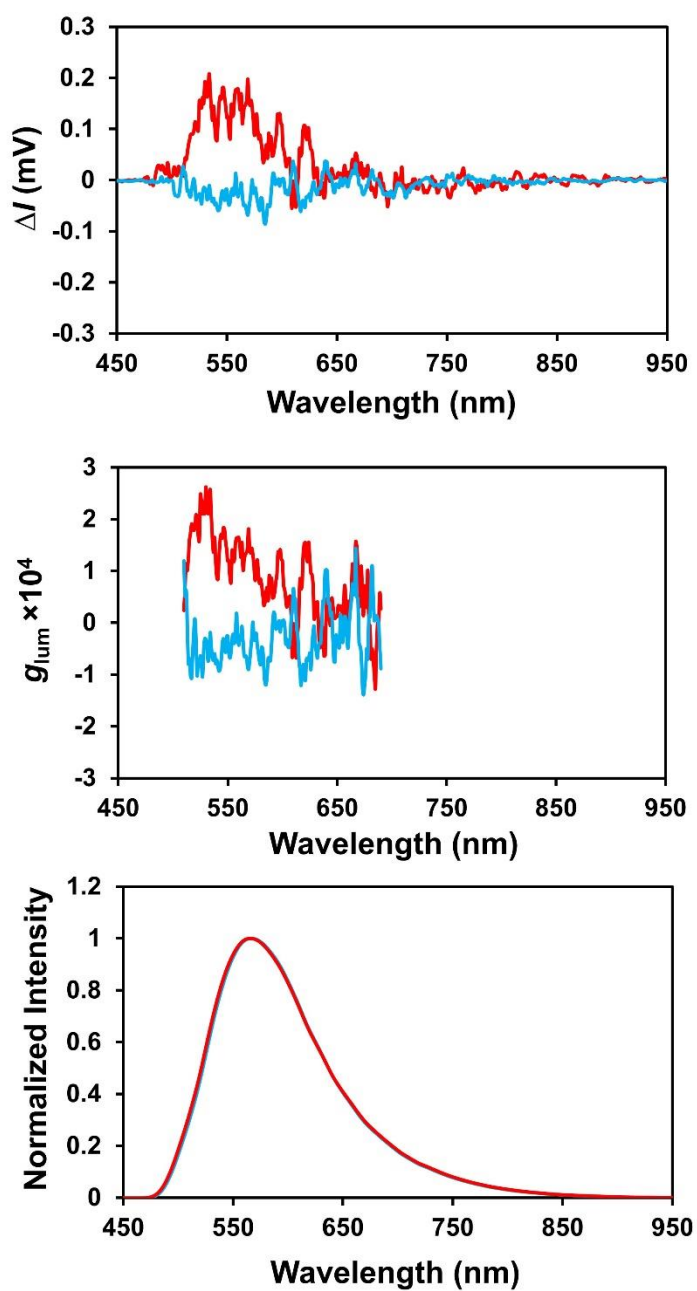
Fig. S20. CPL (top), g_{lum} (middle), and PL (bottom) spectra of (*R*)-**BAmCl** (red) and (*S*)-**BAmCl** (blue) crystalline sample excited at 400 nm.